Journal of Thermal Analysis and Calorimetry (2023) 148:3005–3018
https://doi.org/10.1007/s10973-022-11466-6

Numerical assessment of ceiling-mounted air curtain on the particle distribution in surgical zone

Huiyi Tan[1] · Keng Yinn Wong[2] · Chew Tin Lee[1] · Syie Luing Wong[3] · Bemgba Bevan Nyakuma[4] · Roswanira Abdul Wahab[5] · Kee Quen Lee[6] · Meng Choung Chiong[7] · Wai Shin Ho[1] · Mohd Hafiz Dzarfan Othman[8] · Yat Huang Yau[9] · Hong Yee Kek[2] · Haslinda Mohamed Kamar[2]

Received: 15 December 2021 / Accepted: 19 June 2022 / Published online: 23 July 2022

Abstract
The airflow distribution in an operating room plays a vital role in preventing surgical site infection by diluting and removing particles released by medical staff, lowering particle settlement on a patient. This study aims to computationally examine the efficiency of a ceiling-mounted air curtain in reducing particle distribution in a surgical zone. A computational fluid dynamic (CFD) software simulated an operating room's airflow and particle movements using the corresponding Re-Normalisation Group (RNG) k-ε model and a Lagrangian model. The baseline case and case 1 simulations were equipped with air supply diffusers, while cases 2 to 5 utilised combined air supply diffusers and air curtains. The results revealed that an air curtain fails to reduce particle settlement on a patient. In fact, the use of air curtain in cases 2, 3, 4, and 5 led to an unwanted 3.3-, 4.3-, 3.0-, and 6.7-fold increased particle settlement, respectively. On a positive note, the study found that increasing the area of the air supply diffuser from 4.32 to 7.74 m^2 favourably reduced the number of particles by 33.3%.

Keywords Air curtain · CFD simulation · Particle settlement · Operating room · Air diffuser

Introduction

Surgical site infection (SSI) is defined as an infection on the incision or deep tissue at the surgical site that occurs up to 30 days after surgery [1]. SSI remains a prominent cause of hospital-acquired infection (HAI) [2], accounting for 13–17% and 10–40% of total HAI cases in Europe and the USA, respectively [3]. As a matter of fact, Ling et al. [4] pointed out the alarming high SSI rate in Southeast Asian countries (7.8%) when compared to the USA (0.8%) and Australia (2.8%), thus warranting the development of preventive strategies. SSI is a significant source of healthcare-related infections, leading to additional fatality and healthcare costs related to an extended patient stay in the hospital. A feasible solution to this issue lies in the cleaning maintenance of healthcare facilities, which appreciably differs from conventional cleaning for other built environments. An operating room (OR) demands extensive attention to indoor

✉ Keng Yinn Wong
kengyinnwong@utm.my

1 Faculty of Engineering, School of Chemical & Energy Engineering, Universiti Teknologi Malaysia, 81310 Skudai, Johor, Malaysia

2 Faculty of Engineering, School of Mechanical Engineering, Universiti Teknologi Malaysia, 81310 Skudai, Johor, Malaysia

3 Departamento Matemática Aplicada, Ciencia e Ingeniería de Materiales y Tecnología Electrónica, Universidad Rey Juan Carlos, C. Tulipán, s/n, Móstoles, Madrid, Spain

4 Department of Chemistry, Faculty of Sciences, Benue State University, P.M.B 102119, Makurdi, Benue State, Nigeria

5 Department of Chemistry, Faculty of Sciences, Universiti Teknologi Malaysia, 81310 Skudai, Johor, Malaysia

6 Malaysia-Japan International Institute of Technology, Universiti Teknologi Malaysia Kuala Lumpur, 54100 Kuala Lumpur, Malaysia

7 Faculty of Engineering, Technology & Built Environment, UCSI University, 56000 Cheras, Kuala Lumpur, Malaysia

8 Advanced Membrane Technology Research Centre (AMTEC), Faculty of Engineering, Universiti Teknologi Malaysia, 81310 Skudai, Johor, Malaysia

9 Department of Mechanical Engineering, University of Malaya, 50603 Kuala Lumpur, Malaysia

air cleanliness, wherein a contaminant-free airflow is critical in minimising the risk of exposure of immune-compromised patients to SSI [5].

It has been reported that 98% of the SSI is caused by the particles' settlement on a patient's wound [6] due to the poor airflow distribution in an OR [7]. According to Dascalaki et al. [8], 93% of the particles in the OR are released by medical staff, rendering a sterile procedure inadequate in shielding the patients throughout the surgical procedure. Thus, the ventilation system is vital in ensuring a low particle concentration in the OR environment. Past investigations have proven that appropriate use of airflow reduces the particle concentration at the surgical site [9, 10]. To date, two types of airflow distribution principles are utilised in an OR [11]. The first approach adopts conventional mixing ventilation based on the dilution concept. An OR that utilises mixed ventilation receives an air supply through air diffusers and the air is extracted through exhaust grilles near the floor level. This layout provides a highly mixed airflow in the entire OR by mixing the incoming clean air with the contaminated air in the OR. This ventilation system aims to create an overall low concentration of contaminated air in the OR. The second approach utilises the principle of unidirectional airflow ventilation, where a clean air supply flows from the ceiling towards the surgical site. This creates low turbulence, unidirectional airflow at the surgical site that is less likely to mix with the surrounding air. The unidirectional airflow provides a washing effect over particles present at the surgical zone before leaving the OR through the exhaust grilles. A sufficiently high air change rate from air supply diffusers is pertinent to guarantee a practical washing effect [7].

Apart from the aforementioned ventilation strategies that used to minimize risks of patient contracting the SSIs, Liu et al. [12] further analysed the effectiveness of four different ventilation systems in controlling the bacteria-carrying particles in OR. Observations on airflow field and bacteria-carrying particles phase indicated that obstacles locations in an OR significantly influence the airflow distribution, making it an essential factor in maintaining air cleanliness in the operating area. They found that temperature-controlled ventilation outperformed the three other tested systems. Opening a single sliding door in the OR is another factor that raises the contamination level by 1–10 colony-forming units per cubic meter. However, this issue can be temporarily offset by reducing the OR exhaust flow by 20–30% during door opening [13]. Zhang et al. [14] reported the significant influence of air change rate on the air quality for OR with mixing ventilation. While increasing the air change rate could minimise the SSI risks, medical equipment locations and contamination sources could affect the exhaust efficiency. Laminar flow diffuser size is another factor that impacts the bacteria-carrying particles in an OR. Agirman et al. [15] showed that switching to larger diffuser dimensions from 1.8 m × 2.4 m to 3.2 m × 3.2 m reduces the numbers of 5 µm particle and 20 µm particle by 73 and 32%, respectively. OR size is another factor that deserves attention. Tantillo et al. [16] described those 11,163 patients who underwent orthopaedical surgeries in 2018–2020 showed an increase in SSI incidence from 0.7% in small OR (250–399 net square footage) to 1.8% in large OR (550–699 net square footage). Similarly, the influences of surgeons' body movements and patients' respiratory health [17], exhaust airflows [18], conditions of air filters [19] on the airflow distribution in OR with different ventilation systems were also investigated.

Several studies also demonstrated that using a unidirectional airflow ventilation strategy lowers the patient's risks to SSI [20]. However, Khankari [21] stated that the particles from the surroundings of a surgical zone could re-enter the surgical zone if only fitted with unidirectional airflow ventilation. Lin et al. [22] proposed the application of ceiling return together with a long skirt (a physical barrier mounted on the ceiling) in OR to minimise the likelihood of particle recirculation. However, the presence of a skirt tends to obstruct the movements of medical staff during surgical procedures. Another strategy that uses air curtains to remove particles relies on the ventilation layout design and the operating conditions [21]. Swift et al. [23] suggested that an air curtain installation is required to prevent the penetration of the particles into the surgical zone, resulting from the inhibition of turbulence flow through medical equipment in the OR. However, Zhai, Osborne [24] reported that air curtains reduced particle removal efficiency and increased the particle settlement on a patient. So far, the efficiency of using a combination of unidirectional airflow diffuser and air curtain in an OR remain unclear and warrants further studies by the scientific community. Therefore, this study aims to examine the effectiveness of the ceiling-mounted air curtain in reducing particles concentration in the vicinity of the surgical zone. A CFD model of OR was constructed and validated based on the published data. An RNG k-ε model (turbulence airflow model) was used to simulate the airflow, while a discrete phase model (Lagrangian approach) was used to predict the dispersion of airborne particles. The number of particles settled on a patient was used to evaluate the effectiveness of the ceiling-mounted air curtain.

Methodology

Prescribing airflow and particle conditions

A commercial CFD software, ANSYS Fluent R1 was used to run the airflow and particle dispersion. An RNG k-ε airflow model was used to simulate the airflow in the CFD model of an OR. The reliability of this airflow model has been validated against published data in a patient ward by Zhao

et al. [25]. Both the patient ward and OR have a similar airflow condition and fulfilled the ISO 14644 [26] classification cleanroom. They utilised the ceiling-mounted unidirectional air supply diffuser and the low-level exhaust grilles. Both rooms had positive pressurisation over the adjacent regions. The governing equations for the RNG k-ε model are given by Eqs. 1 and 2 [27, 28]:

$$\frac{\partial}{\partial t}(\rho k)+\frac{\partial}{\partial x_i}(\rho k u_i)=\frac{\partial}{\partial x_j}\left(\alpha_k \mu_{\text{eff}}\frac{\partial k}{\partial x_j}\right)+G_k+G_b+\rho\varepsilon-Y_M+S_k \tag{1}$$

and

$$\frac{\partial}{\partial t}(\rho\varepsilon)+\frac{\partial}{\partial x_i}(\rho\varepsilon u_i)=\frac{\partial}{\partial x_j}\left(\alpha_\varepsilon \mu_{\text{eff}}\frac{\partial \varepsilon}{\partial x_j}\right)+C_{1\varepsilon}\frac{\varepsilon}{k}(G_k+C_{3\varepsilon}G_b)-C_{2\varepsilon}\rho\frac{\varepsilon^2}{k}-R_{\varepsilon+}S_\varepsilon \tag{2}$$

where ρ is the fluid density, t is time, ε is the turbulent dissipation, k is turbulent kinetic energy, u_i is the velocity component, x_i is the coordinate, μ_{eff} is the effective viscosity, G_k represents the generation of turbulent kinetic energy due to mean velocity gradients, G_b is the generation of turbulent kinetic energy due to buoyancy, Y_M is the contribution of the fluctuating dilatation in the compressible turbulence to the overall dissipation rate, and S_k and S_ε are user-defined source term. $C_{1\varepsilon}$ and $C_{2\varepsilon}$ are model constants, used by default as 1.42 and 1.68, respectively. R_ε is the additional term in ε equation, α_k and α_ε are the Prandtl numbers for k and ε, both with a value of 1.393 [27].

This study employed a pressure-based segregated algorithm based on the assumption that the air in the OR is incompressible. The simulations were performed under a steady-state condition with a second-order upwind discretisation scheme. The second-order scheme aids in reducing the effects of numerical diffusion on the solution to improve the simulation accuracy [29]. A SIMPLE algorithm was utilised to couple the velocity and pressure [30]. The convergence criterion for the simulation was targeted at 1×10^{-4} for the equations of turbulent kinetic energy, turbulent dissipation, x-velocity, y-velocity, z-velocity, and continuity, while 1×10^{-9} was set for the energy equation. These values were chosen based on the suggestion in the literature [3, 31].

In predicting particle dispersion, gravitational and drag forces were considered in the simulation. Both forces have a significant effect on micro-sized particles [32]. Also, shear lift force and thermophoresis force have been included in this study. The purpose is to provide a reliable prediction of temperature gradient and shear at near wall region. Brownian diffusivity was excluded in the study as the effect on submicron particles is negligible [33]. The discrete random walk (DRW) model was also considered to simulate the effect of the stochastic air velocity fluctuations [29]. The DRW model predicts the air velocity fluctuation based on Gaussian probability distribution. The equation that expressed the force balance equation of the discrete phase model is given in Eq. (3) [27]:

$$\frac{\mathrm{d}u_p}{\mathrm{d}t}=F_D(u-u_p)+g\left(1-\frac{\rho}{\rho_p}\right)+\frac{2Kv^{\frac{1}{2}}\rho d_{ij}}{\rho_p d_p(d_{lk}d_{kl})}(u-u_p)-\frac{6\pi d_p\mu^2 C_s(K+C_tKn)}{\rho(1+3C_mKn)(1+2K+2C_tKn)m_oT}\nabla T \tag{3}$$

where $F_D\ u_p)$ represents the drag force, $\frac{2Kv^{1/2}\rho d_{ij}}{\rho_p d_p(d_{lk}d_{kl})}(u-u_p)$ represents the shear lift force, $\frac{-6\pi d_p\mu^2 C_s(K+C_tKn)}{\rho(1+3C_mKn)(1+2K+2C_tKn)m_oT}\nabla T$ represents the thermophoretic force, u_p is particle velocity, g is the gravitational force, ρ is the fluid density, ρ_p is particle density, d_p is the diameter of particle, d_{ij} is the deformation tensor, Kn is the Knudsen number, $K=k/k_p$, k is fluid thermal conductivity, k_p is the particle thermal conductivity, T is local fluid temperature, m_p is the particle mass, μ is the fluid viscosity, and C_s, C_t, and C_m are constants with values 1.17, 2.18, and 1.14, respectively.

Description and boundary settings of CFD model of baseline and case studies

The CFD model of the baseline case OR has a dimension of 6 m × 5.5 m × 3 m (length × width × height), which belongs to a private hospital in Kelantan, Malaysia (6.1254°N, 102.2381°E). The OR was equipped with a ceiling-mounted air supply diffuser, six low-level exhaust grilles, two surgical lamps, one operating table, two medical equipment, and an equipment table. The detailed dimensions of each item are retrieved from Kamar et al. [3]. Five upright medical staff members were placed around a patient lying down on the operating table in the OR. These positions are commonly utilised in previous studies, which mimic a surgical procedure in progress [34]. Heat flux values of 116 and 58 W m^{-2} were specified on the medical staff member and patient, respectively [35]. The heat flux specified on the patient is lower than the medical staff due to no physical performance was performed [3]. Figure 1 shows the CFD model of a baseline case OR that was fully furnished, occupied by the medical staff members and a patient.

Clean air is supplied from the ceiling-mounted air supply diffuser, and the air is then removed from the OR via the six low-level exhaust grilles. The air in the OR was

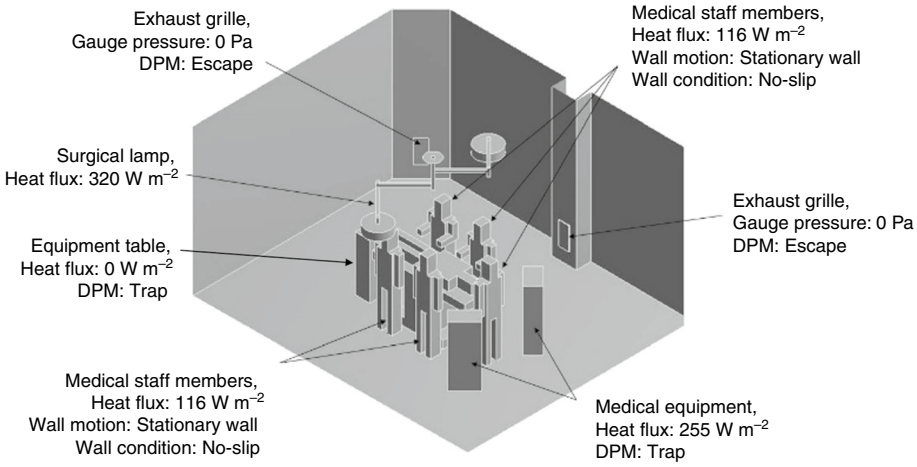

Fig. 1 CFD model of a baseline case OR with detailed boundary conditions

considered to have an average temperature of 19 °C, with a density of 1.208 kg m^{-3}. Other simulated factors include the specific heat of 1.005 kJ kg^{-1} K, the thermal conductivity of 0.0256 W m^{-1} K, and kinematic viscosity of 15.02×10^{-6} $m^2 s^{-1}$. The air supply diffuser has a total surface area of 4.32 m^2, while each exhaust grille has a surface area of 0.10 m^2. Each medical staff member is assumed wearing cleanroom clothing. Rui et al. [36] set the release rate as 400 particles/min person (lower body) and 200 particles/ min person (upper body), Liu et al. [37] set the release rate as 600 particles/ min person (mainly from upper body), Chow, Yang [38] set the release rate as 100 particles/min person, while Hu [39] measured the release rate as 681 particles/min person. So far, there is no consensus on the exact value of the particle release by medical staff. As the focus of this study is to evaluate the efficiency of ventilation strategy and not the particle release rate with respect to the body part. Present study considered the particles were released at a rate of 600 particles/min (equivalent to 1.31×10^{-12} kg s^{-1}), equally distributed from the medical staff's body surfaces. Although particles with sizes ranged 5 to 10 µm show significant correlation with the infectious particle, the difference in dispersion characteristics of airborne particles for 5 to 10 µm were claimed to be negligible under a low turbulent condition [36, 37]. Hence, the present study has chosen the size of 5 µm to represent the infectious particles. Each particle has an aerodynamics size of 5 µm, with a density of 2.001 g cm^{-3} [37]. The present study assumed there is no penetration of particles into the OR via the air supply diffuser. The reason is that the air supply diffusers were equipped with a HEPA type-E filtration system, which has a 99.97% trapping efficiency towards the particles with a diameter larger than 0.3 µm [40].

A total of five case studies were considered in this investigation. The baseline case and case 1 referred to a ceiling-mounted air supply diffuser without the air curtain, but the latter has a larger air supply diffuser's area. Cases 2 and 3 have identical air supply diffuser and air curtain layouts, but the air curtain in case 3 supplies a higher air velocity. Cases 4 and 5 also have similar air supply diffuser and air curtain layouts, except for case 5, which uses a higher air velocity air curtain. All the layouts design fulfilled the requirements of an OR, as stated in ASHRAE Standard [41]. The baseline case, case 1, case 2, case 3, case 4, and case 5 have an air change rate of 67 h^{-1}, 121 h^{-1}, 185 h^{-1}, 209 h^{-1}, 197 h^{-1}, 223 h^{-1}, respectively. The air supply diffuser and air curtain layouts for the baseline and 5 case studies are shown in Fig. 2, while the descriptions are tabulated in Table 1.

Meshing and verifying the grid independency

The CFD model of the OR was discretised with unstructured tetrahedral elements. The fine mesh option that yielded small elements was used at regions with a high gradient of airflow changes, i.e. air supply diffuser, exhaust grilles, surgical lamps, medical staff members, patients, and medical equipment. The coarse mesh option that yielded larger elements was utilised at other regions in the CFD model of the OR. The smallest and the largest mesh elements that utilised in the CFD model are 0.0012 and 0.0102 m, respectively. A growth rate of 1.2 that resulted in a 20% increment in element edge length was used to provide a uniform growth of elements size [42]. It is important to note that a proper growth rate selection could help achieve desired mesh skewness and aspect ratio. Although they found that a 10-inflation layer setup might enhance the prediction at the viscous sublayer [43], the present study found that the relative difference between 5 and 10 layers was less than 1%. This finding corresponded to a study by Fawwaz Alrebi et al. [42], who also performed a low turbulence airflow analysis in the healthcare facility. Therefore, the present study utilised this setup on all walls in the CFD model, aiming to improve the airflow prediction at the boundary layers [42]. The description of the mesh setup is shown in Fig. 3.

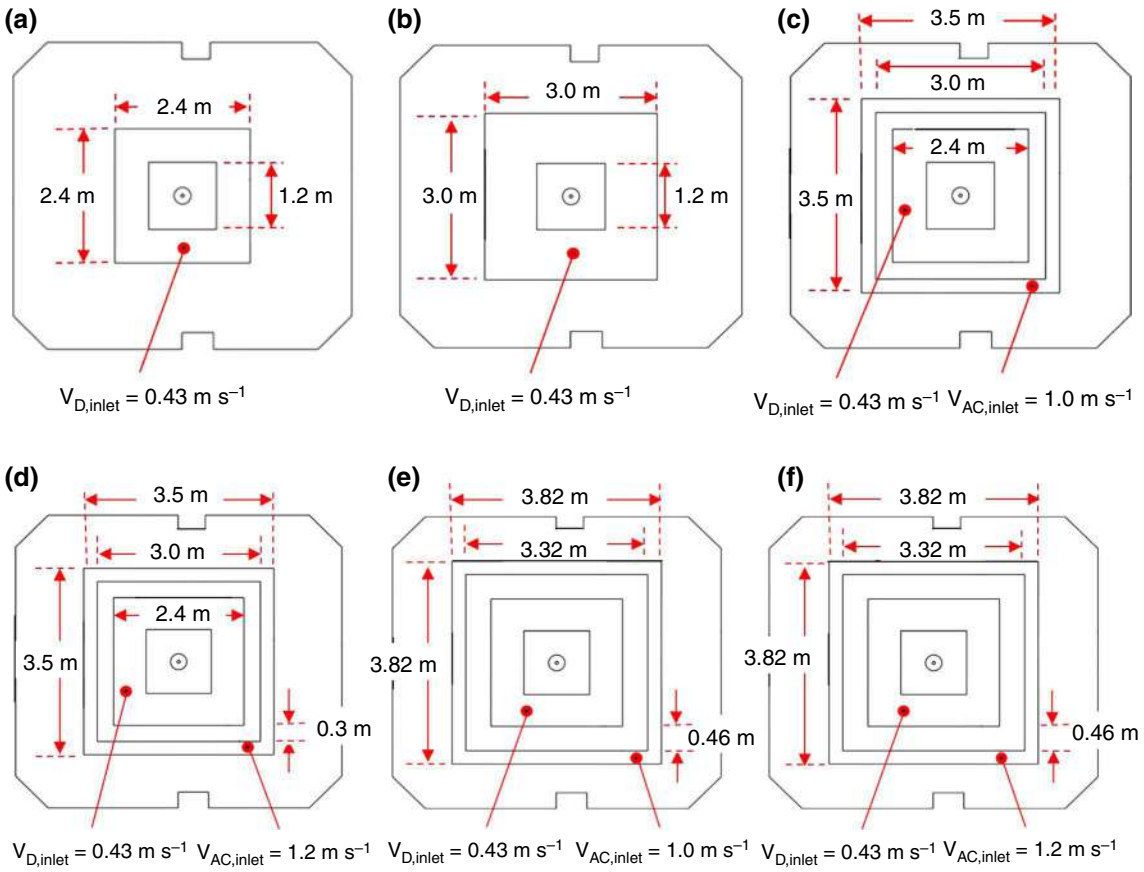

Fig. 2 Plan view of air supply diffuser and air curtain layouts for baseline and case 1, case 2, case 3, case 4, and case 5*$V_{D,inlet}$ and $V_{AC,\ inlet}$ denote air velocity supplied from air diffuser and air curtain, respectively

Table 1 Setup of air supply diffuser and air curtain for the baseline and 5 case studies

Case	Air supply diffuser				Air curtain			
	Velocity/m s^{-1}	Effective area/m^2	Turbulent intensity/%	Reynolds Number	Velocity/m s^{-1}	Effective area/m^2	Turbulent intensity/%	Reynolds Number
Baseline	0.43	4.32	5	3.44×10^4	–	–	–	–
1	0.43	7.74	5	5.15×10^4	–	–	–	–
2	0.43	4.32	5	3.44×10^4	1.0	3.25	10	3.33×10^4
3	0.43	4.32	5	3.44×10^4	1.2	3.25	10	3.99×10^4
4	0.43	4.32	5	3.44×10^4	1.0	3.57	10	3.33×10^4
5	0.43	4.32	5	3.44×10^4	1.2	3.57	10	3.99×10^4

Based on the GIT result as shown in Fig. 4 a, b and c, the variation of air velocity using 1,000,000, 2,000,000, 4,000,000, and 8,000,000 was insignificant. While based on the GCI calculation, the values were 7.1%, 4.0%, 3.3%, and 2.3% for 1,000,000 2,000,000, 4,000,000, and 8,000,000 elements, respectively. This GCI result showed that the CFD model required at least 2,000,000 elements to achieve grid independence (GCI < 5%). Therefore, 2,000,000 elements were used on the CFD model of baseline and all five case studies. A reduced GCI with increasing elements indicated that the air velocity prediction does not lead to divergence. To ensure that the mesh densities are fine, the non-dimensional distance (y^+) was controlled in the range of $1 \le y^+ \le 6$ throughout the entire CFD model of the OR, as described by an earlier study by Agirman et al. [30].

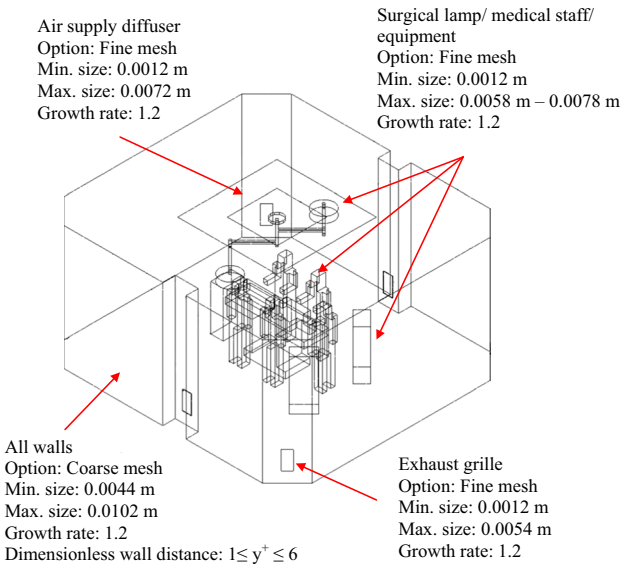

Fig. 3 Mesh details applied on the CFD model of the OR

Validation of CFD model

Validation of the CFD model was performed by comparing the simulated results with published data. The purpose of validation is to ensure that the simulation procedures are appropriate, and the simulated results are reliable. The data published by Zhao et al. [25] were chosen for validation as the indoor condition is highly similar to the present case study. The simulation was performed under a steady-state condition, which means all the variables in the analysis are independent of time. A Computer-Aided Design (CAD) software was used to construct the CFD model of a patient ward with the dimension of 3.3 m × 3.1 m × 2.5 m (length × width × height), as shown in Fig. 5.

The CFD model was discretised with 1,200,000 unstructured tetrahedral elements, as chosen based on the Grid Independent Test (GIT) and Grid Convergence Index (GCI). Unstructured tetrahedral elements are reliable in both complex and straightforward CFD models [44]. GIT was done to identify the minimum number of element numbers in achieving mesh independence by simulating with a coarse mesh set before further refinement using a finer set of mesh. This procedure is repeated until the variation of airflow velocities is less than 5% between two sets of the refined mesh [45]. The variation of airflow velocities was plotted along the x-axis and z-axis lines, connecting the coordinates of 0.00, 0.80, 0.72, and 3.30, 0.80, 0.72 as well as 1.65, 0.80, 0.00 and 1.65, 0.80, 3.10, respectively. The GIT for this CFD model of a patient ward is shown in Fig. 6.

GCI was also calculated to determine the meshing uncertainty. The mesh is deemed adequately fine when a GCI value falls below 5% [34]. A GCI could be calculated based on Eq. (4) [29]:

$$\mathrm{GCI}(u) = \frac{F_s \varepsilon_{\mathrm{rms}}}{r^p - 1} \tag{4}$$

where F_s is the safety factor, with a value of 3, $\varepsilon_{\mathrm{rms}}$ is the relative difference between subsequent solutions, r is the ratio of the number of the fine elements to that of coarse elements, and p is the convergence's order, with a value of 2 [29]. The safety factor F_s is arbitrarily set based on the accumulated experience in CFD simulations [46]. It represents 95% confidence for the estimated error band [47]. The $\varepsilon_{\mathrm{rms}}$ could be defined based on Eq. (5) [3]:

$$\varepsilon_{\mathrm{rms}} = \sqrt{\frac{\sum_{i=1}^{n} \frac{\left(u_{\mathrm{i,\,coarse}} - u_{\mathrm{i,\,fine}}\right)^2}{u_{\mathrm{i,\,fine}}}}{n}} \tag{5}$$

where u_i is the airflow velocity. Based on the calculation, the GCI for 600,000 elements, 1,200,000 elements and 2,400,000 elements were 7.6%, 3.7%, and 1.5%, respectively. Hence, 1,200,000 elements are selected as the GCI is less than 5%. Although 2,400,000 elements could yield a smaller GCI, the effect on the predicted result is insignificant. In contrast, the use of 2,400,000 elements will significantly increase the computational time.

The Reynolds number at the air supply diffuser inlets in all cases is greater than 20,000, therefore the turbulence generated by the ventilation system cannot be ignored [48]. In this validation section, four airflow turbulence models that developed based on the Reynolds-Averaged Navier–Stokes (RANS) equations were used to simulate the airflow condition in the patient ward. These RANS turbulence models are standard k-ε, RNG k-ε, standard k-ω, and SST k-ω, which were reported reliable in airflow prediction in a low turbulence indoor environment [3]. Among these four models, the airflow velocities predicted by RNG k-ε have the best fit the measured airflow velocities. Based on the calculated result, the relative error between the measured and predicted airflow velocities using the RNG k-ε model is 9.62%. However, the standard k-ε, SST k-ω, and standard k-ω have a relative error of 10.55%, 11.20% and 10.81%, respectively. Since the RNG k-ε model error is less than 10%, it can be construed that the CFD model airflow results were valid [3]. The relative error percentage was estimated via Eq. (6) [3].

$$\text{Relative error} = \frac{\text{Measurement value} - \text{Simulated value}}{\text{Measurement value}} \tag{6}$$

The comparison of airflow velocities predicted by the RNG k-ε model and measured by Zhao et al. [25] along lines L1, L2, and L3 is shown in Fig. 7. The lines L1, L2, and L3 connected the coordinates (0.00, 1.20, 0.65) and (3.30, 1.20,

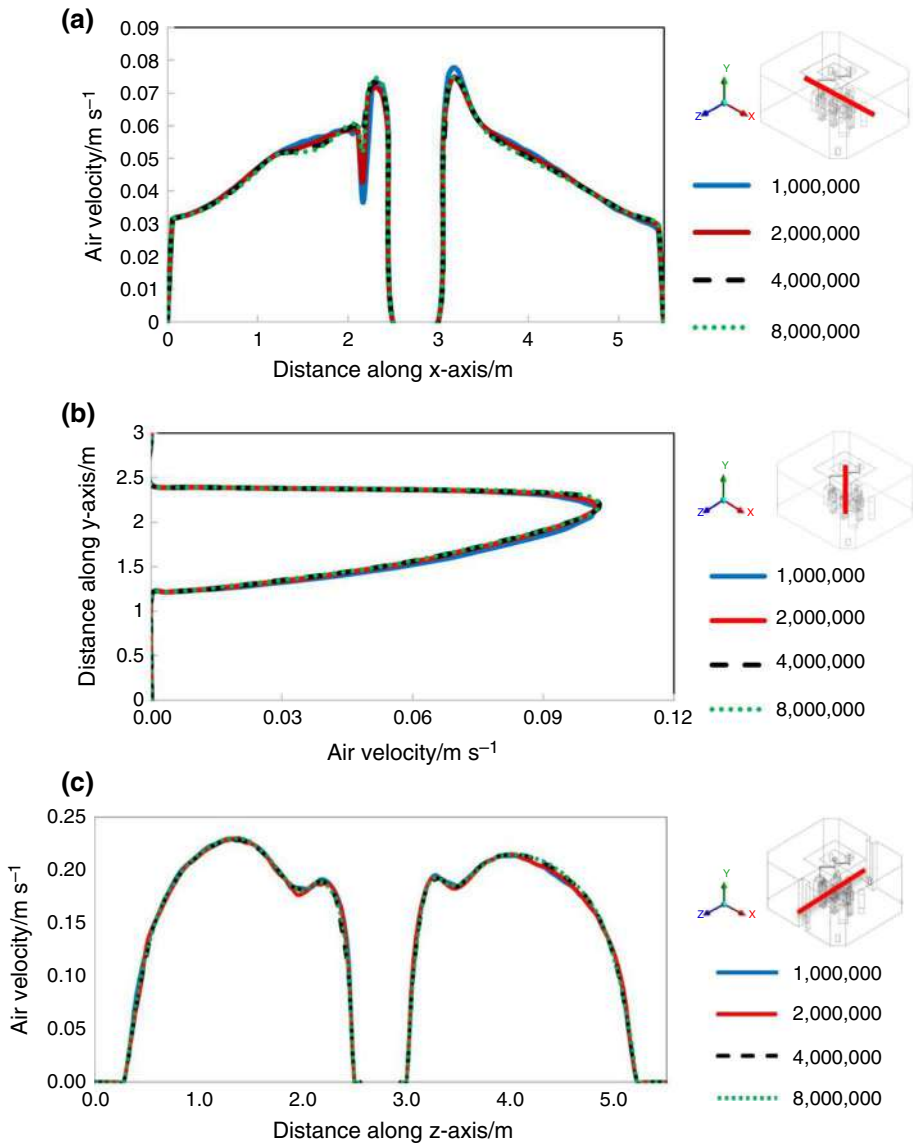

Fig. 4 Variation of air velocity along the (**a**) x-axis line, (**b**) y-axis line, and (**c**) z-axis line in the OR

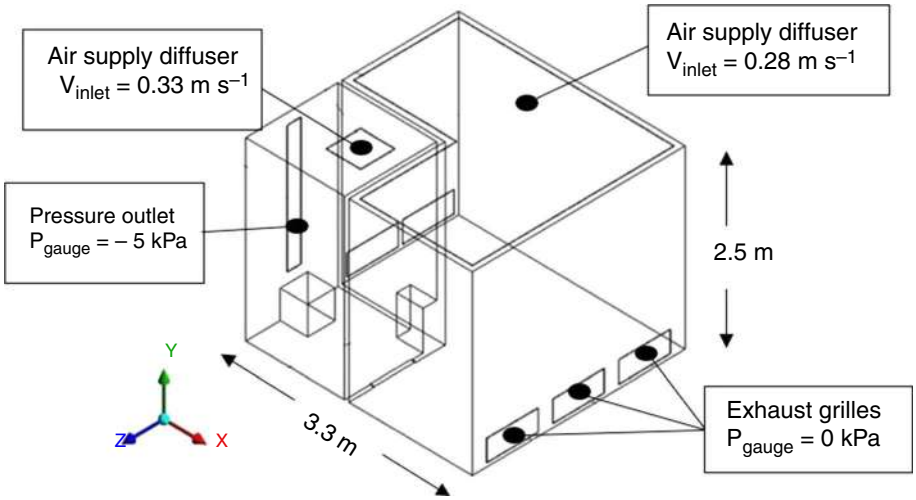

Fig. 5 Boundary conditions prescribed on the CFD model of a patient ward

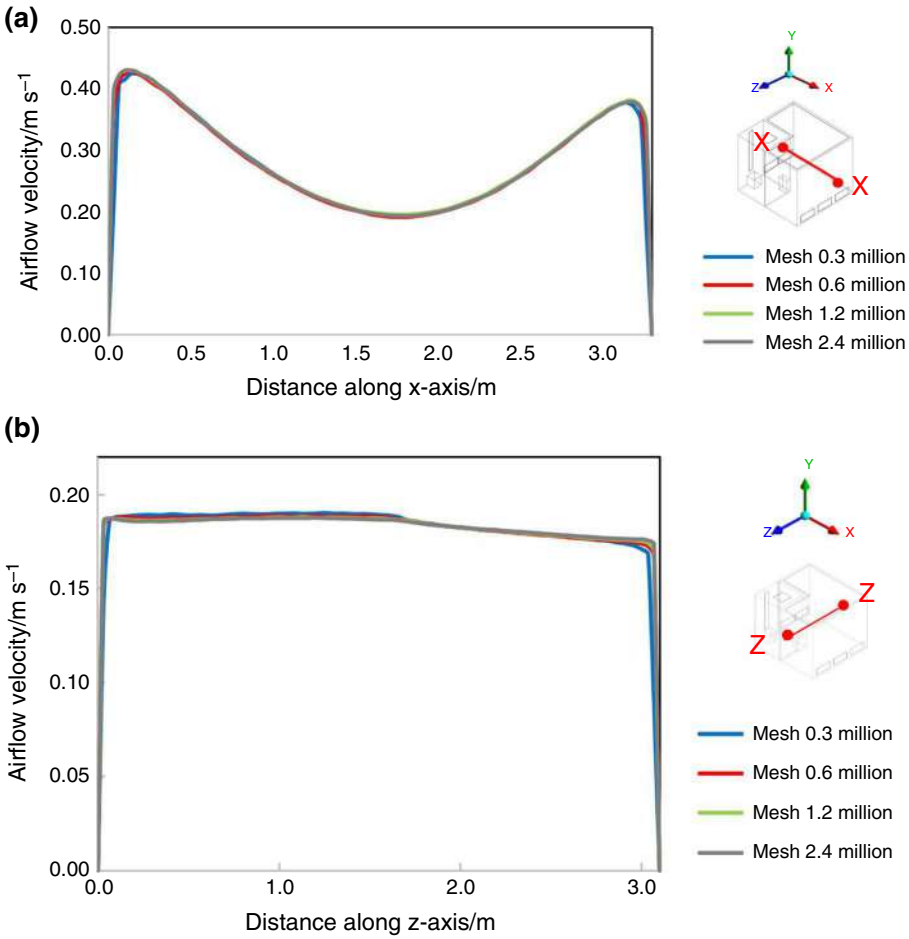

Fig. 6 Variation of airflow velocities along the (**a**) x-axis line, and (**b**) z-axis line

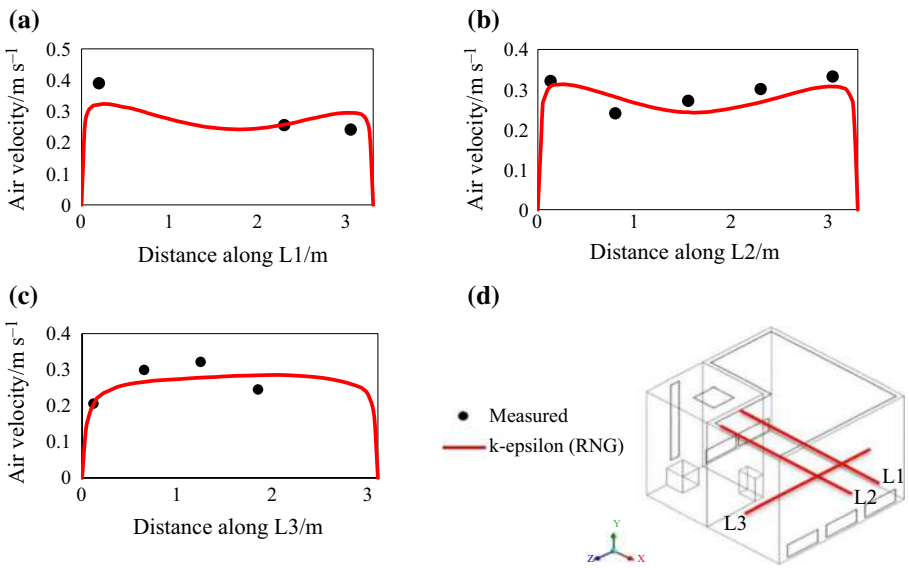

Fig. 7 Air velocities plotted along the lines (**a**) L1, (**b**) L2, (**c**) L3; (**d**) indicator of lines L1, L2, and L3

0.65), (0.00, 1.20, 1.25) and (3.30, 1.20, 1.25), and (2.40, 1.20, 0.00) and (2.40, 1.20, 3.10), respectively.

A validation on the particle distribution in the patient ward was performed to ensure the simulated particle results are reliable. The particle tracking method was based on the Lagrangian approach. The particle concentration along five lines, namely lines P1, P2, P3, P4 and P5 were performed. A good agreement between measured

and simulated particle concentration result was found, where the mean relative error was approximately 7.3%. Only one point along line P4 has a larger error, which due to the particle device leakage during onsite measurement [25]. The dimensionless particle concentration that displays in Fig. 7 can be defined using Eq. (7) [49].

$$C_{\text{dim}} = \frac{C}{C_{\text{ref}}} \tag{7}$$

where C_{dim} is dimensionless concentration, C is local particle concentration, and C_{ref} is reference particle concentration (concentration at height of 0.8 m on line P5). The comparison of the predicted particle concentration and measured particle concentration along lines P1, P2, P3, P4, and P5 is shown in Fig. 8.

Results and discussion

Airflow velocity distribution

Based on the present study, the airflow velocity distribution in the baseline case OR was the lowest, with the average velocity distribution on the y-plane = 1.1 m at 0.16 m s^{-1}. While the airflow velocity distribution in case 5's OR was the highest. The average velocity distribution on the plane

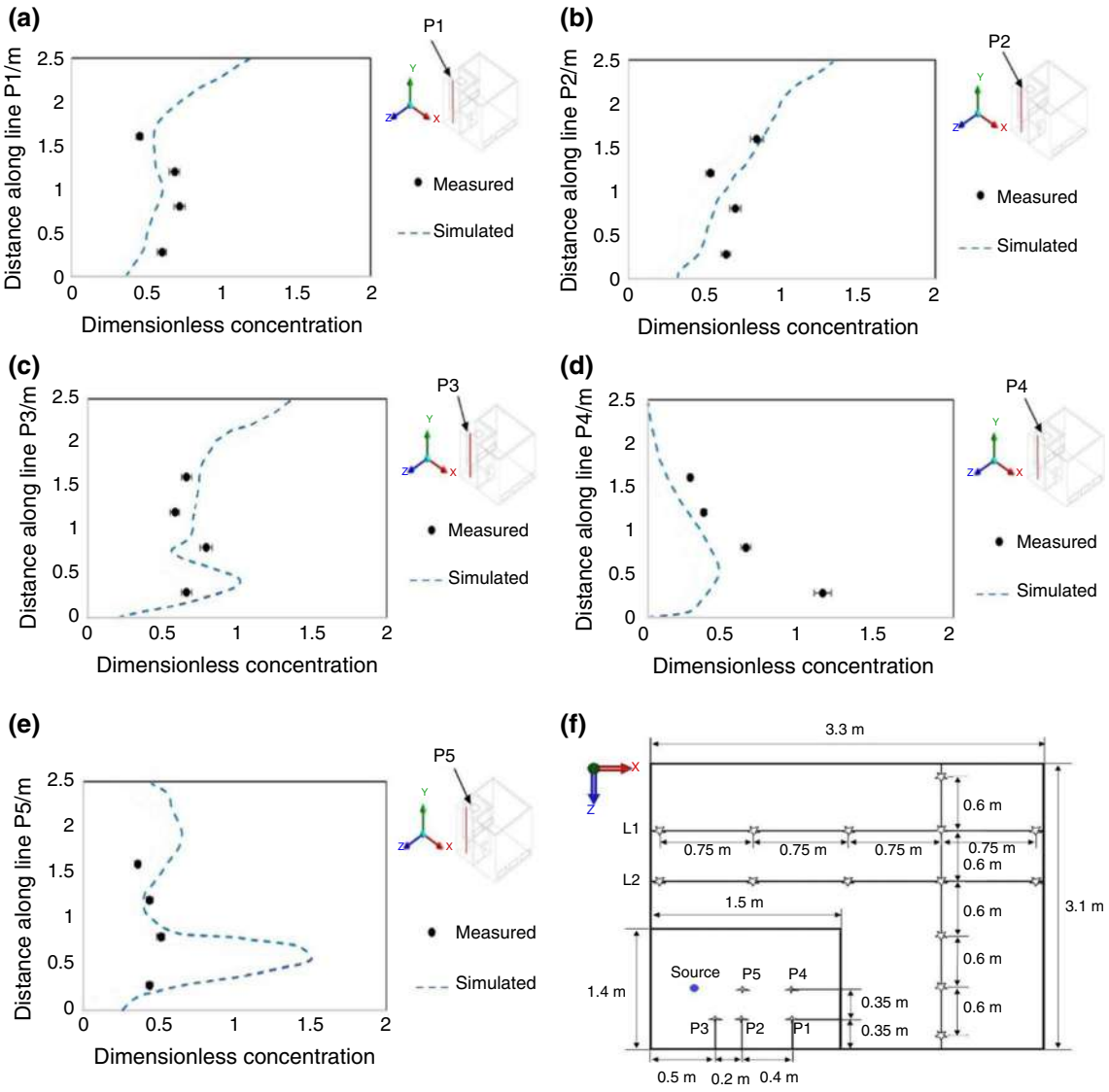

Fig. 8 Dimensionless particle concentration plotted along the lines (**a**) P1, (**b**) P2, (**c**) P3, (**d**) P4, (**e**) P5, (**f**) indicator of lines P1, P2, P3, P4, and P5

of $y = 1.1$ m was 0.34 m s^{-1}, approximately twice the average air velocity of the baseline case. The air volume flow rates supplied in the OR for the baseline case 1, case 2, case 3, case 4, and case 5 are 1.86 m^3 s^{-1}, 3.33 m^3 s^{-1}, 5.11 m^3 s^{-1}, 5.76 m^3 s^{-1}, 5.41 m^3 s^{-1}, and 6.12 m^3 s^{-1}, respectively. These values are determined based on the air supplied from the ceiling-mounted air supply diffuser and air curtain. The airflow velocity distribution in the OR for different case studies is shown in Fig. 9.

Referring to Fig. 9c–f, the air curtain supplied a higher air velocity into the OR, which directly contributes to a higher air change rate. The purpose of using the air curtain is to provide a better dilution and higher removal efficiency towards the particle concentration. Also, it can act as an air barrier to prevent the particles from surrounding flow into the vicinity of surgical zone, which due to the recirculating airflow. However, the study discovered that the high-velocity airflow from the air curtain disrupted the vertically downward airflow from the air supply diffuser, causing more particles to disperse around the medical staff members and flow into the vicinity of the surgical zone. Also, the vertically downward uniform airflow that supplied from the air diffuser tended to combine with the high velocity air supplied from the air curtain (due to the lower pressure region). This phenomenon has led the airflow to move in the diagonally outward direction, and causing a stagnant airflow condition in the surgical zone. The stagnant airflow region (airflow velocity is close to zero) can be identified at the region nearby medical staff members and patient, as shown in Fig. 9c–f.

Particle concentration

Under the baseline case and case 1 ORs (as shown in Fig. 10a, b), the air supplied from the ceiling-mounted air supply diffuser provides the washing effect over particles released by the medical staff members. The particles largely moved downward along with the airflow from the ceiling-mounted air supply diffuser. A noticeable stagnant region existed under the two surgical lamps following an obstructed airflow from the ceiling-mounted air supply diffuser. However, the particles did not remain trapped in this region as nearly all particles were dispersed at a height lower than 1.8 m above floor level. The particle distribution that cut through the two medical staff members on the x-plane = 2.8 m is shown in Fig. 10.

As observed from Fig. 10c–f, the air supplied from the air curtain has increased the airflow velocity distribution and turbulent intensity in the OR. When the air passed through the obstacles, separation and swirling flows were identified at the regions nearby to medical lamps, staff members, and below the operating table. A notable particle concentration of approximately 28 particles m^{-3} is identified in the case studies equipped with the air curtain (Fig. 10c–f). The current study showed that airflow from the air curtain did not dilute the particle concentration effectively but served as an

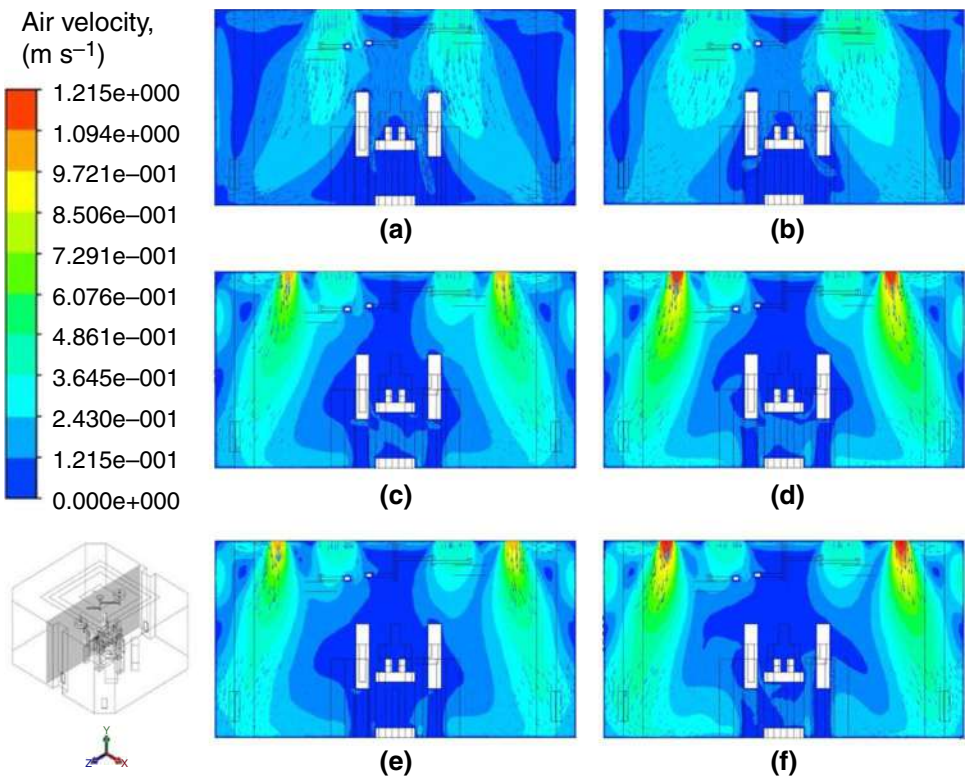

Fig. 9 Airflow velocity distribution cut through the x-plane = 2.8 m for (**a**) baseline case, (**b**) case 1, (**c**) case 2, (**d**) case 3, (**e**) case 4, (**f**) case 5

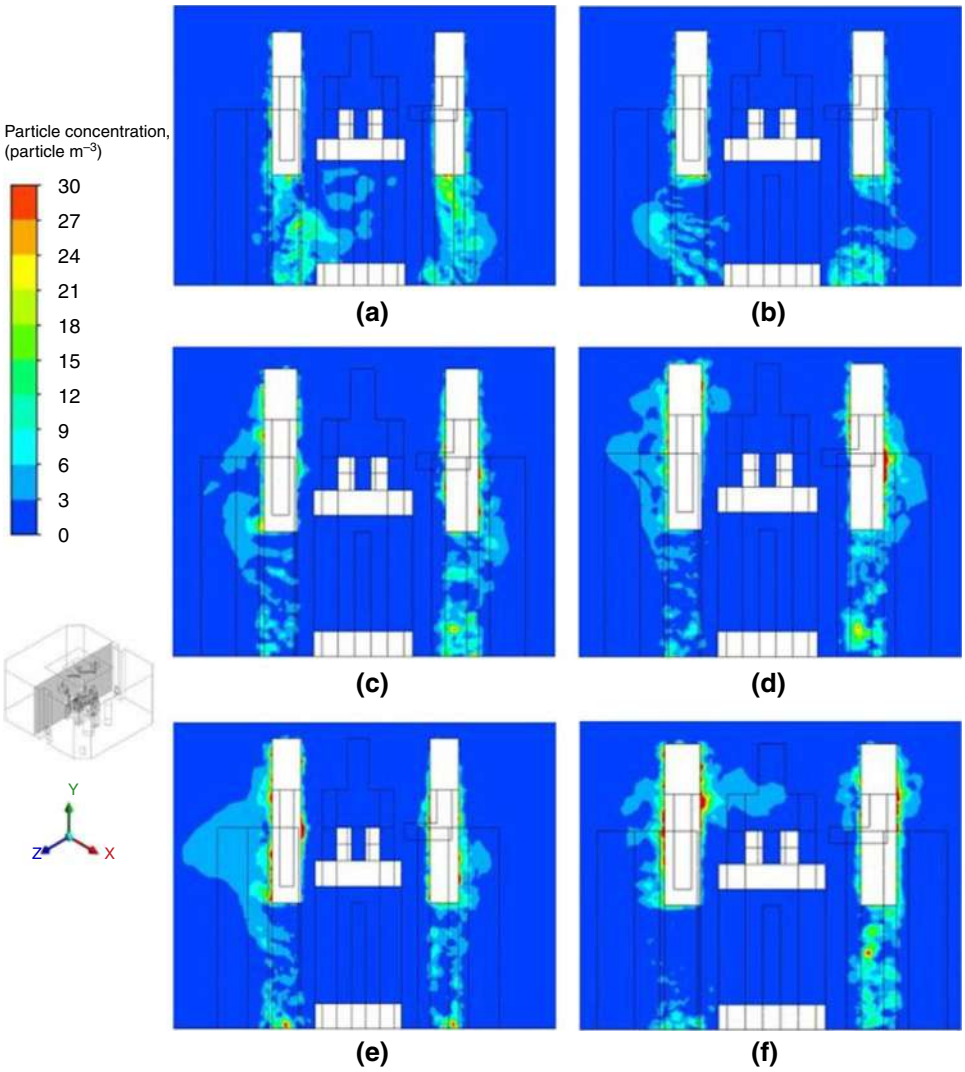

Fig. 10 Variation of particle concentration cut through the *x*-plane = 2.8 m for (**a**) baseline case, (**b**) case 1, (**c**) case 2, (**d**) case 3, (**e**) case 4, (**f**) case 5

air barrier that restricted particle removal from the surgical zone. Comparing both ORs that did not equip with an air curtain (baseline and case 1), case 1 (larger air supply diffuser) can remove more particles from the surgical zone than the baseline case. Particles notably accumulated between gaps in the leg of staff in the baseline case. However, the study showed that downward moving particles were less likely to accumulate in the upper body region.

The present study also proven that a higher airflow rate supply into the room does not necessary reduce the particle concentration in the room. Based on the current ventilation configuration in the OR, a higher airflow rate has promoted more particle dispersed in an unpredictable manner, which due to the non-unidirectional airflow. It is expected that a combination of strategic air supply diffuser placement and a high airflow rate could improve the particle removal efficiency from the surgical zone. Such verification required a well-design study in the near future. Figure 11 shows the particle dispersion due to the air curtain could be observed from the plan view at 1.5 m above floor level height.

As shown in Fig. 11, the ORs equipped with the air supply diffuser (i.e. the baseline and case 1) performed the worst, showing a maximum particles concentration of 13 particles m^{-3} trapped at the upper body of medical staff members. In contrast, the ORs (i.e. cases 2–5) with the air supply diffuser and air curtain have a maximum particle concentration of 27 particles m^{-3} trapped at the upper body of medical staff members. Likewise, the particles could disperse to a horizontal distance up to 1.26 m. Such particle dispersion pattern is not desirable in a surgical zone due to a higher possibility of flowing into the patient's vicinity and settling on the wound. This could subsequently increase the tendency of the patient to contact an SSI.

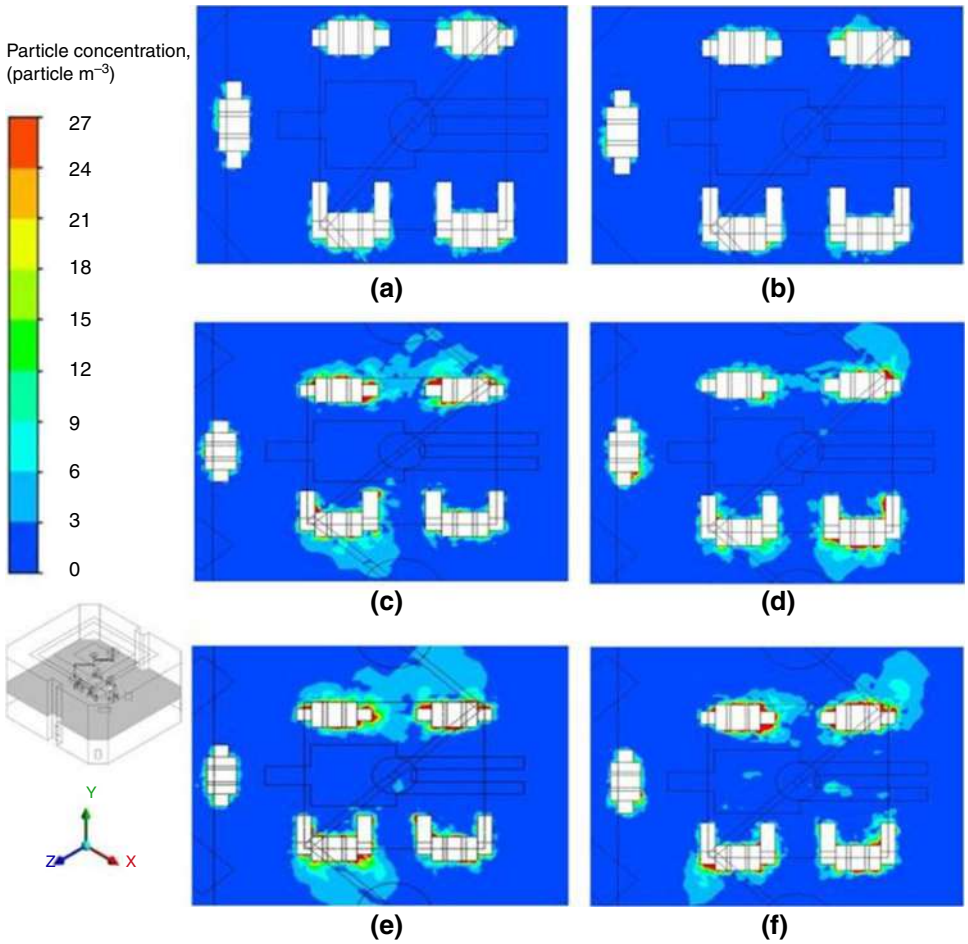

Fig. 11 Variation of particle concentration cut through the *y*-plane = 1.5 m for (**a**) baseline case, (**b**) case 1, (**c**) case 2, (**d**) case 3, (**e**) case 4, (**f**) case 5

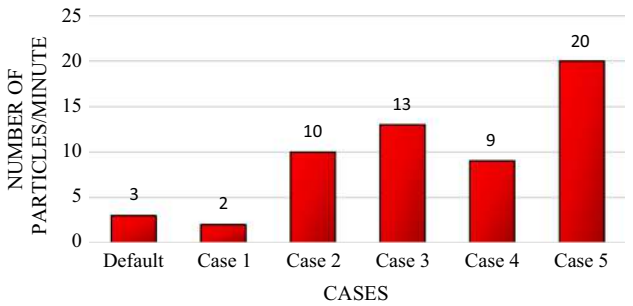

Fig. 12 Number of particles settled on the patient in one minute under baseline and case studies

Deposition of particle numbers on patient

As shown in Fig. 12, case 1 is the best-case scenario, showing the lowest number of particles settled on a patient. This result indicated that a larger air supply diffuser could reduce the particle settlement by 33.3%. The elevated unidirectional clean air in the OR effectively removed the particles released by the medical staff members, but in case 5 (the OR equipped with air supply diffuser and air curtain), particle settlement was increased by 6.7-fold. Although cleaner air is supplied to the OR, the airflow characteristics adversely reduce the particle removal efficiency. The current study has a good consensus with the findings of Zhai, Osborne [24]. However, the air supply diffuser layout utilised in their study is a full panel diffuser placed above the patient, compared to the perimeter-type layout used in this study. Zhai, Osborne [24] further justified extending the air supply diffuser area from 2.97 to 7.46 m^2 could achieve zero particle settlement on the patient's wound.

Conclusions and recommendations

A CFD approach was used to simulate the airflow and particle dispersion in an operating room to establish the effectiveness of ceiling-mounted air curtains in reducing the settlement of particles on a surgical patient. Among the four turbulence models, the RNG k-ε was the most appropriate for predicting the airflow in an OR. The present study showed that using an air curtain did not reduce the number of particles that settle on a patient. The air curtain was found to interrupt the downward airflow from the air supply diffuser. This

scenario subsequently caused the particles to disperse into the vicinity of the surgical zone. However, the presence of an air curtain (in cases 2–5) increased particle settlement from threefold to sevenfold, while increasing the ceiling-mounted air supply diffuser's area from 4.32 to 7.74 m^2, favourably reducing particle settlement on a patient by 33.3%.

Present study disregards the human's movement into the analysis. Human's movement could potentially induce secondary airflow that interferes with particle dispersion and increase the patient's risks to SSI. Such consideration could reflect medical staff member behaviours during the surgical procedures. Also, present study assumed the particles were evenly released from the medical staff surfaces, and there are no particles were released from the sources out of the surgical zone. In the future studies, it is recommended to incorporate the medical staff member's movement, design a thorough study on the particle release rate with respect to body part, and include other particles sources in the airflow and particle dispersion analysis. Another interesting aspect of further improving the prediction of particle dispersion is to consider the photophoretic force. Currently, the default option of integrating the photophoresis force is not available in most commercial CFD software. Hence, a proper design study on developing a user-defined function (UDF) that accounts for the photophoresis force would be a good future study.

Supplementary Information The online version contains supplementary material available at https://doi.org/10.1007/s10973-022-11466-6.

Acknowledgements The authors would like to acknowledge the Ministry of Education (MOE) through Fundamental Research Grant Scheme (FRGS/1/2020/TK0/UTM/02/42) provided for this study. This research was also financially supported by the Mini Research Grant by Institution of Mechanical Engineers (IMechE), Malaysia Branch, under the Vot No. 4C587.

Authors' contribution Conceptualization, methodology, funding acquisition, and writing of original draft were contributed by KYW. conceptualization, methodology, and writing of original draft were contributed by HT, CTL, SLW; methodology and reviewing were contributed by BBN, KQL, MCC, HMK, HYK; methodology, editing, reviewing, and funding acquisition were contributed by WSH. writing—review and editing, were contributed by RAW, MHDO, YYH.

References

1. Owens CD, Stoessel K. Surgical site infections: epidemiology, microbiology and prevention. J Hosp Infect. 2008;70(Suppl 2):3–10. https://doi.org/10.1016/s0195-6701(08)60017-1.
2. McDonald S, Bott A. Surgical site infections. Surg Infect (Larchmt). 2020;38(3):150–4. https://doi.org/10.1016/j.mpsur.2020.01.001.
3. Kamar HM, Wong KY, Kamsah N. The effects of medical staff turning movements on airflow distribution and particle concentration in an operating room. J Build Perform Simul. 2020;13(6):684–706. https://doi.org/10.1080/19401493.2020.1812722.
4. Ling ML, Apisarnthanarak A, Abbas A, Morikane K, Lee KY, Warrier A, et al. APSIC guidelines for the prevention of surgical site infections. Antimicrob Resist Infect Control. 2019;8:174. https://doi.org/10.1186/s13756-019-0638-8.
5. Brock-Utne JG, Ward JT, Jaffe RA. Potential sources of operating room air contamination: a preliminary study. J Hosp Infect. 2021;113:59–64. https://doi.org/10.1016/j.jhin.2021.04.020.
6. Chauveaux D. Preventing surgical-site infections: Measures other than antibiotics. Orthop Traumatol Surg Res. 2015;101(1, Supplement):S77–83. https://doi.org/10.1016/j.otsr.2014.07.028.
7. Knudsen RJ, Knudsen SMN, Nymark T, Anstensrud T, Jensen ET, La Mia Malekzadeh MJ, et al. Laminar airflow decreases microbial air contamination compared with turbulent ventilated operating theatres during live total joint arthroplasty: a nationwide survey. J Hosp Infect. 2021;113:65–70. https://doi.org/10.1016/j.jhin.2021.04.019.
8. Dascalaki EG, Lagoudi A, Balaras CA, Gaglia AG. Air quality in hospital operating rooms. Build Environ. 2008;43(11):1945–52. https://doi.org/10.1016/j.buildenv.2007.11.015.
9. Wagner JA, Greeley DG, Gormley TC, Markel TA. Comparison of operating room air distribution systems using the environmental quality indicator method of dynamic simulated surgical procedures. Am J Infect Control. 2019;47(1):e1–6. https://doi.org/10.1016/j.ajic.2018.07.020.
10. Sadeghian P, Wang C, Duwig C, Sadrizadeh S. Impact of surgical lamp design on the risk of surgical site infections in operating rooms with mixing and unidirectional airflow ventilation: a numerical study. J Build Eng. 2020. https://doi.org/10.1016/j.jobe.2020.101423.
11. Wang C. Ventilation Performance in operating rooms: a numerical assessment: KTH royal institute of technology; 2019.
12. Liu Z, Liu H, Yin H, Rong R, Cao G, Deng Q. Prevention of surgical site infection under different ventilation systems in operating room environment. Front Environ Sci Eng. 2020;15(3):36. https://doi.org/10.1007/s11783-020-1327-9.
13. Wang C, Holmberg S, Sadrizadeh S. Impact of door opening on the risk of surgical site infections in an operating room with mixing ventilation. Indoor and Built Environ. 2019;30(2):166–79. https://doi.org/10.1177/1420326X19888276.
14. Zhang Y, Cao G, Feng G, Xue K, Pedersen C, Mathisen HM, et al. The impact of air change rate on the air quality of surgical microenvironment in an operating room with mixing ventilation. J Build Eng. 2020;32:101770. https://doi.org/10.1016/j.jobe.2020.101770.
15. Agirman A, Cetin YE, Avci M, Aydin O. Effect of laminar airflow unit diffuser size on pathogen particle distribution in an operating room. Sci Technol Built Environ. 2021;27(4):402–13. https://doi.org/10.1080/23744731.2020.1816405.
16. Tantillo T, Petrone B, Stapleton E, Frane N, Matai P, Lutsky L, et al. The effect of operating room size on orthopaedic surgical site infection rates. J Am Acad Orthop Surg. 2021. https://doi.org/10.5435/jaaos-d-20-01022.
17. Li H, Zhong K, Zhai Z. Investigating the influences of ventilation on the fate of particles generated by patient and medical staff in operating room. Build Environ. 2020;180:107038. https://doi.org/10.1016/j.buildenv.2020.107038.
18. Xue K, Cao G, Liu M, Zhang Y, Pedersen C, Mathisen HM, et al. Experimental study on the effect of exhaust airflows on the surgical environment in an operating room with mixing ventilation. J Build Eng. 2020;32:101837. https://doi.org/10.1016/j.jobe.2020.101837.
19. Pereira ML, Vilain R, Kawase PR, Tribess A, Morawska L. Impact of filtration conditions on air quality in an operating room. Int

J Environ Res. 2020;14(6):685–92. https://doi.org/10.1007/s41742-020-00286-x.
20. Andersson AE, Petzold M, Bergh I, Karlsson J, Eriksson BI, Nilsson K. Comparison between mixed and laminar airflow systems in operating rooms and the influence of human factors: experiences from a Swedish orthopedic center. Am J Infect Control. 2014;42(6):665–9.
21. Khankari K. Hospital operating room ventilation systems. ASHRAE J. 2018;60(6):16–26.
22. Lin T, Zargar OA, Lin K-Y, Juiña O, Sabusap DL, Hu S-C, et al. An experimental study of the flow characteristics and velocity fields in an operating room with laminar airflow ventilation. J Build Eng. 2020;29:101184. https://doi.org/10.1016/j.jobe.2020.101184.
23. Swift J, Avis E, Millard B, Lawrence TM. Air distribution strategy impact on operating room infection control. In: Proceedings of the Clima, Citeseer; 2007.
24. Zhai Z, Osborne AL. Simulation-based feasibility study of improved air conditioning systems for hospital operating room. Front Arch Res. 2013;2(4):468–75. https://doi.org/10.1016/j.foar.2013.09.003.
25. Zhao B, Yang C, Chen C, Feng C, Yang X, Sun L, et al. How Many airborne particles emitted from a nurse will reach the breathing zone/body surface of the patient in iso class-5 single-bed hospital protective environments? A numerical analysis. Aerosol Sci Technol. 2009;43(10):990–1005. https://doi.org/10.1080/02786820903107925.
26. Standard ISO. ISO 14644–1, Cleanrooms and associated controlled environments. Classification of air cleanliness. United Kingdom: Institute of Environmental Sciences and Technology; 1999.
27. Fluent A. Ansys fluent theory guide. ANSYS Inc USA. 2011;15317:724–46.
28. Mozafarie SS, Javaherdeh K, Ghanbari O. Numerical simulation of nanofluid turbulent flow in a double-pipe heat exchanger equipped with circular fins. J Therm Anal Calorim. 2021;143(6):4299–311. https://doi.org/10.1007/s10973-020-09364-w.
29. Wong K, Kamar H, Kamsah N. Enhancement of airborne particles removal in a hospital operating room. Int J Automot Mech Eng. 2019;16(4):7447–63.
30. Agirman A, Cetin YE, Avci M, Aydin O. Effect of air exhaust location on surgical site particle distribution in an operating room. Build Simul. 2020;13(5):979–88. https://doi.org/10.1007/s12273-020-0642-1.
31. Eslami J, Abbassi A, Saidi M. Numerical simulation of the effect of visitor's movement on bacteria-carrying particles distribution in hospital isolation room. Sci Iran Trans B Mech Eng. 2017;24(3):1160.
32. Tao Y, Inthavong K, Tu J. Computational fluid dynamics study of human-induced wake and particle dispersion in indoor environment. Indoor Built Environ. 2016;26(2):185–98. https://doi.org/10.1177/1420326x16661025.
33. Zhang Z, Chen Q. Comparison of the Eulerian and Lagrangian methods for predicting particle transport in enclosed spaces. Atmos Environ. 2007;41(25):5236–48. https://doi.org/10.1016/j.atmosenv.2006.05.086.
34. Wong KY, Haslinda MK, Nazri K, Alia SN. Effects of surgical staff turning motion on airflow distribution inside a hospital operating room. Evergreen. 2019;6(1):52–8.
35. Sadrizadeh S, Afshari A, Karimipanah T, Håkansson U, Nielsen PV. Numerical simulation of the impact of surgeon posture on airborne particle distribution in a turbulent mixing operating theatre. Build Environ. 2016;110:140–7. https://doi.org/10.1016/j.buildenv.2016.10.005.
36. Rui Z, Guangbei T, Jihong L. Study on biological contaminant control strategies under different ventilation models in hospital operating room. Build Environ. 2008;43(5):793–803. https://doi.org/10.1016/j.buildenv.2007.01.018.
37. Liu J, Wang H, Wen W. Numerical simulation on a horizontal airflow for airborne particles control in hospital operating room. Build Environ. 2009;44(11):2284–9. https://doi.org/10.1016/j.buildenv.2009.03.019.
38. Chow T-T, Yang X-Y. Performance of ventilation system in a non-standard operating room. Build Environ. 2003;38(12):1401–11. https://doi.org/10.1016/S0360-1323(03)00155-0.
39. Hu Z. Study on bacteria emission rate of human body and relationship of deposited bacteria and suspending bacteria in air. Tianjin University: Tianjin University; 1988.
40. Tan H, Wong KY, Nyakuma BB, Kamar HM, Chong WT, Wong SL, et al. Systematic study on the relationship between particulate matter and microbial counts in hospital operating rooms. Environ Sci Pollut Res Int. 2022;29(5):6710–21. https://doi.org/10.1007/s11356-021-16171-9.
41. Standard ASHRAE. Standard 62, Ventilation for acceptable indoor air quality. Ventilation for acceptable indoor air quality. USA: ASHRAE; 2010. p. 51.
42. Fawwaz Alrebi O, Obeidat B, Atef Abdallah I, Darwish EF, Amhamed A. Airflow dynamics in an emergency department: a CFD simulation study to analyse COVID-19 dispersion. Alex Eng J. 2021. https://doi.org/10.1016/j.aej.2021.08.062.
43. Li W, Chong A, Hasama T, Xu L, Lasternas B, Tham KW, et al. Effects of ceiling fans on airborne transmission in an air-conditioned space. Build Environ. 2021;198:107887. https://doi.org/10.1016/j.buildenv.2021.107887.
44. Haţiegan C, Răduca M, Frunzăverde D, Răduca E, Pop N, Gillich GR. The modeling and simulation of the thermal analysis on the hydrogenerator stator winding insulation. J Therm Anal Calorim. 2013;113(3):1217–21. https://doi.org/10.1007/s10973-013-3089-0.
45. Wulandari DA, Akmal M, Gunawan Y. Cooling improvement of the IT rack by layout rearrangement of the A2 class data center room: a simulation study. Evergreen. 2020;7(4):489–99.
46. Kwaśniewski L. Application of grid convergence index in FE computation. Bull Pol Acad Sci Tech Sci. 2013;61(1):123–8.
47. Sadrizadeh S, Holmberg S, Nielsen PV. Three distinct surgical clothing systems in a turbulent mixing operating room equipped with mobile ultraclean laminar airflow screen: a numerical evaluation. Sci Technol Built Environ. 2016;22(3):337–45.
48. Alicandro ACD, Mauro A. Effects of operating room layout and ventilation system on ultrafine particle transport and deposition. Atmos Environ. 2021;2022(270):118901. https://doi.org/10.1016/j.atmosenv.2021.118901.
49. Yang C, Yang X, Xu T, Sun L, Gong W. Optimization of bathroom ventilation design for an ISO Class 5 clean ward. Buil Simul. 2009. https://doi.org/10.1007/s12273-009-9310-1.